Electronic Supplementary Material (ESI) for Nanoscale.
This journal is © The Royal Society of Chemistry 2016

Supporting Information

Passivated Ambipolar Black Phosphorus Transistor

Dewu Yue[1], Daeyeong Lee[1], Young Dae Jang[1], Min Sup Choi[1], Hye Jin Nam[2], Duk-Young Jung[2] and Won Jong Yoo[1*]

1. SKKU Advanced Institute of Nano-Technology (SAINT), Samsung-SKKU Graphene/2D Center (SSGC), Department of Nano Science and Technology, Sungkyunkwan University (SKKU), 2066, Seobu-ro, Jangan-gu, Suwon, Gyeonggi-do, 16419 Korea.
2. Department of Chemistry, Sungkyunkwan University, 2066, Seobu-ro, Jangan-gu, Suwon, Gyeonggi-do, 16419 Korea

*Corresponding author: yoowj@skku.edu

This material contains: S1-S9; Table S1-S4, Supplementary Note 1

S1

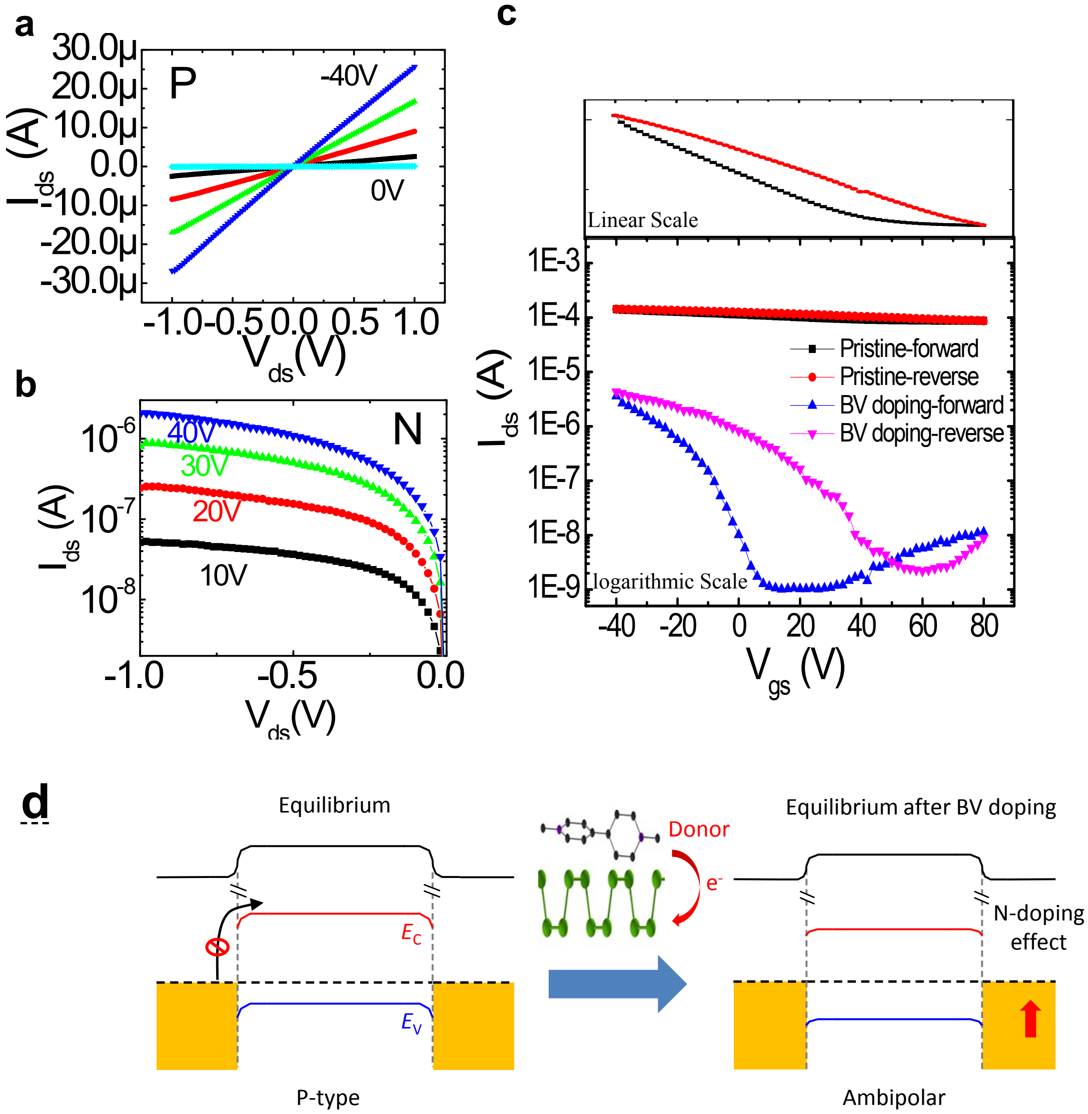

Figure S1 | **a,b,** Transfer characteristics of the BP field effect transistor (BV1) before and after BV doping. **c,** Hysteresis before and after BV doping. After doping, BV on BP surface induce scattering, which causes larger hysteresis than the pristine state. **d,** band diagram of the pristine and BV-doped BP FETs under equilibrium.

S2

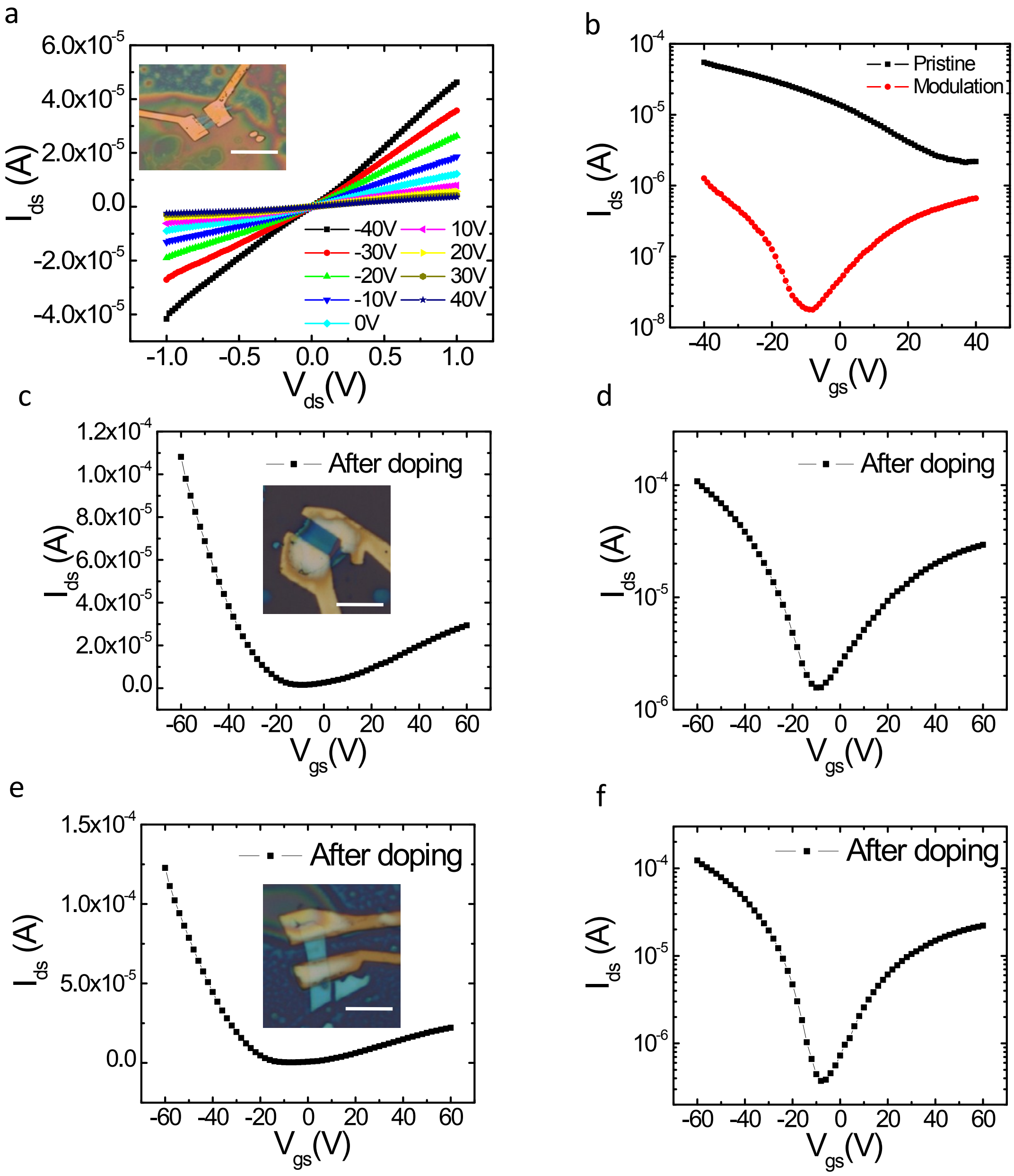

Figure S2 a, Output characteristics of BP field effect transistor (BV2) **b** and **c, d, e,** show the transfer characteristics (I_{ds}-V_{gs}) of BP device (BV2, BV3, BV4) after BV doping in linear and logarithmic scale. The scale bar indicates 5 µm.

S3

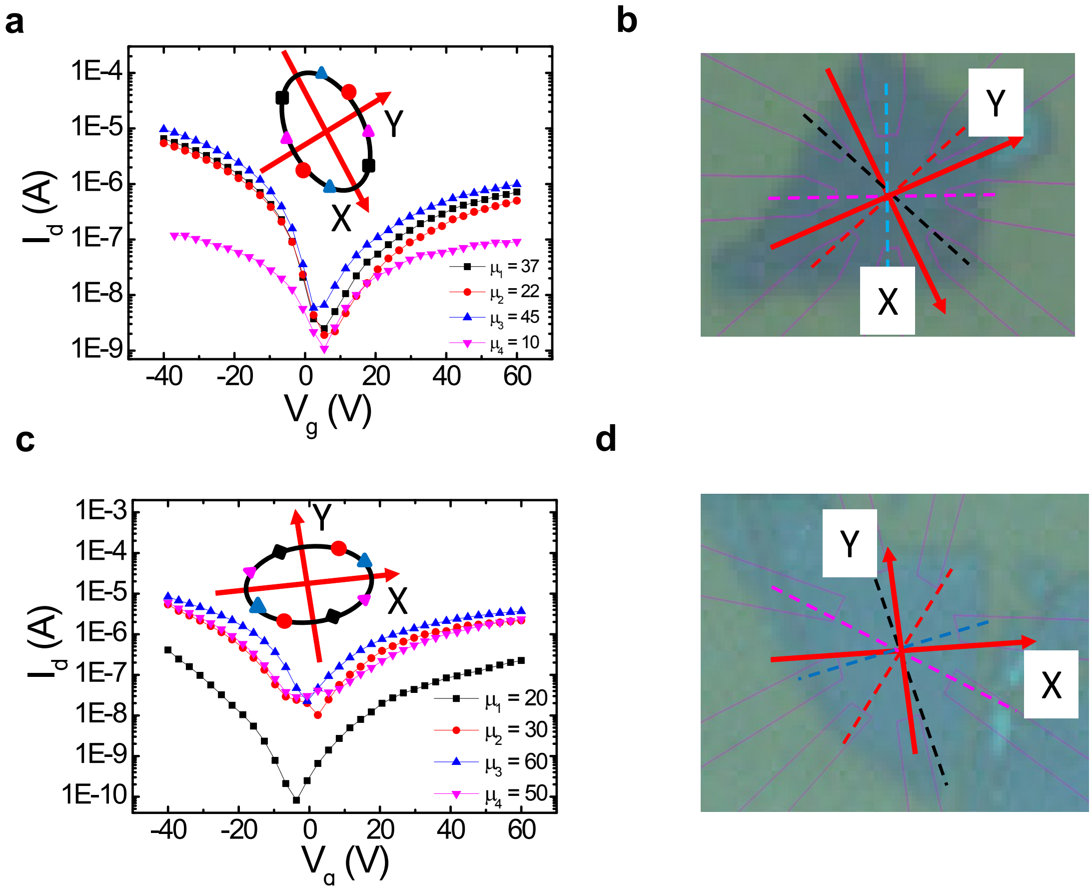

Figure S3 | a, c, Output characteristics of BP field effect transistor in different directions. The curves show electron mobilities (μ) with different colors. It can be seen that the electrons transport along x- direction is higher than y- direction, because of the different effective mass. **b, d,** Optical microscope image with marked with x- and y- direction from the mobility results.

Table S1

Table S1 | Performance parameters of devices after BV doping.

Samples*	**Mobility (cm^2/Vs)**		**I_{On}/I_{off}**	**Thickness (nm)**
	Pristine	**After BV doping**		

	Hole	Hole	Electron		
BV1	176	91	28	10^3	8
BV2	101	20	5	10^2	6
BV3	330	260	83	10^2	10
BV4	320	280	34	10^2	15

*BV# denotes the BP FET device fabricated by BV doping.

Table S2

Table S2 | Performance Characteristics of recent works.

Strategy	**Mobility (cm^2/V s)** Pristine Hole	Modulated Hole	Modulated Electron	**On / off**	***T* (K)**	**Ref**
BV doping	330	260	82	10^2	273	This work
MoO_3 or Cs_2CO_3 doping	215	-	27	10^4	273	Ref. [1]
hBN passivation	118	86	62	10^2	200	Ref. [2]
Al_2O_3 capping	-	172	38	10^3	273	Ref. [3]
Gr electrode and hBN capping	-	120	40	-	273	Ref. [4]
Encapsulated on flexible polyimide afforded	-	310	90	10^3	273	Ref.[5]

T is measurement temperature; Gr means graphene.

S4

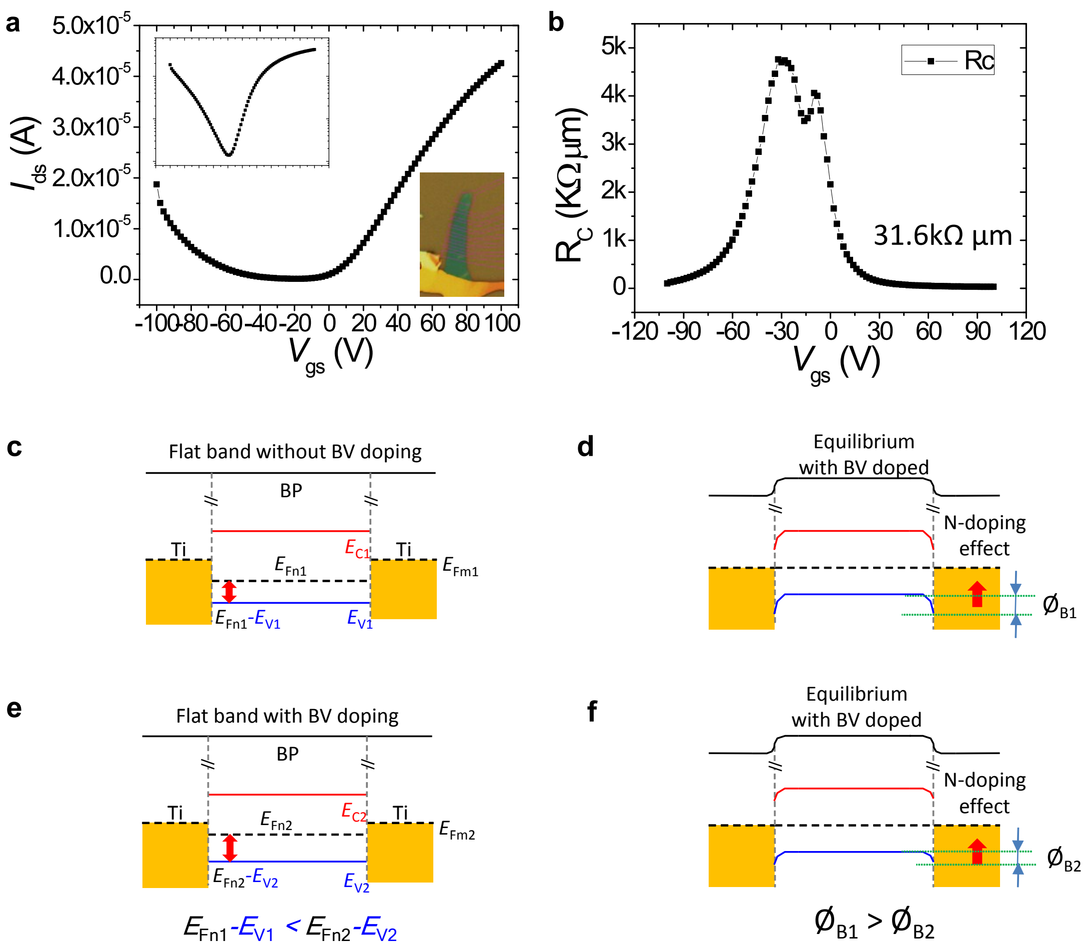

Figure S4 | N-type BP FETs and mechanism. a, The source-drain current as a function of gate voltage. **b,** The contact resistance as a function of gate voltage. **c** and **d**, Band diagrams when the doping was performed only on channel. **e** and **f**, Band diagram when the doping was performed both on the channel and beneath the metal.

Figure S4 c shows the flat band without BV doping, comparing to Figure S4 e, which shows the flat band with BV doping. It can be seen that Fermi level (E_{Fn2}) of BV doped BP is more close to the conduction band, because of BV doping effect. So, E_{Fn1}-E_{V1} < E_{Fn2}-E_{V2}. When we deposit metal on BP flake, it significantly affects the formation of Schottky barrier. Figure b and d show the equilibrium state of two cases. Due to the difference in Fermi level, the Schottky barrier height is different between two cases. The Schottky barrier height (SBH) in BV doped both at the channel and beneath the metal of BP FETs is smaller than another one. Thus, $\varnothing_{B2} < \varnothing_{B1}$. It is known that Schottky barrier is closely related to contact resistance. The relation $\log(Rc) \propto SBH$ can be used in this case. That is, when Schottky barrier height is small, there should be small contact resistance between metal and semiconductor, as shown in Figure S4 b.

Table S3

Time (hour)	$V_{cnp\ (neutral\ point)}$ (V)	$\mu_{P,\ max}$ (cm^2/V s)	$\mu_{n,\ max}$ (cm^2/V s)	$I_{ds,\ p\ (\triangle Vgs=\ -\ 90\ V)}$ (μA)	$I_{ds,\ n\ (\triangle Vgs=\ +\ 90V)}$ (μA)
47.3	-10	208	24	74-	21
48.1	-10	206	23	77	21
48.3	-10	210	23	76	21
48.8	-10	203	24	76	21
49.8	-12	211	23	81	21
51.8	-10	205	22	77	22
54.1	-12	211	25	82	22
62.1	-12	205	20	83	21
86.1	-12	220	20	86	20
94.6	-8	220	23	77-	22
108.1	-10	207	23	81	20
113.1	-10	214	22	80	18
118.6	-10	220	24	82	20
130.6	-8	202	23	81	17
141.6	-8	220	22	84	16
154.1	-6	219	20	77	15
161.6	-4	222	22	75-	15
167.6	-6	212	20	76	16
177.6	-6	215	18	79	14
231.5	-10	170	18	85	13
239.6	0	185	14	81	15
250.1	6	185	14	74	12

Table S3 | Air-stable characteristics vs time. V_{cnp} is the charge neutral point, $\mu_{P,\ max}$ is the maximum mobility for holes, and $\mu_{n,\ max}$ is the maximum mobility for electrons. $I_{ds,\ p\ (\triangle Vgs=\ -\ 90\ V)}$ is the source-drain current at V_{gs}= - 90 V, $I_{ds,\ n\ (\triangle Vgs=\ +\ 90V)}$ is the source-drain current at V_{gs} = 90 V.

S5

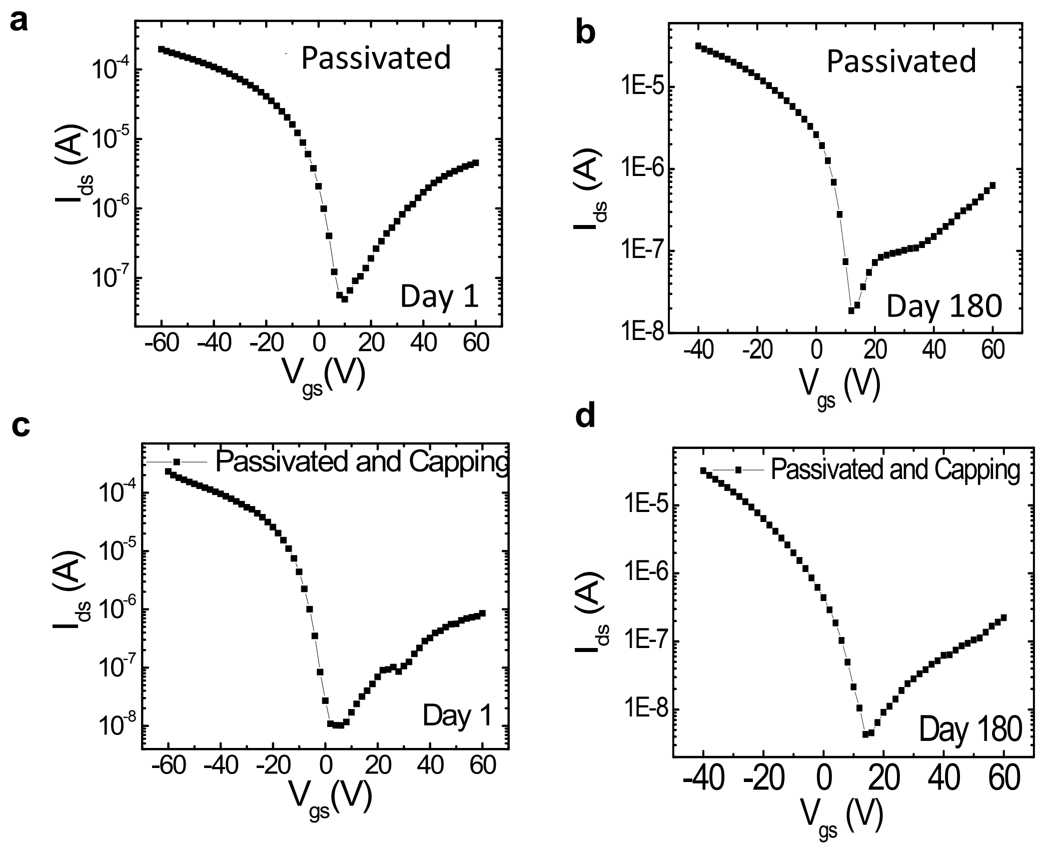

Figure S5 | **a, b,** Output characteristics of BV passivated BP field effect transistor after exposing to the air for 180 days. **c, d,** Output characteristics of BP field effect transistor with both BV passivated and h-BN capped after exposing to the air for 180 days.

S6

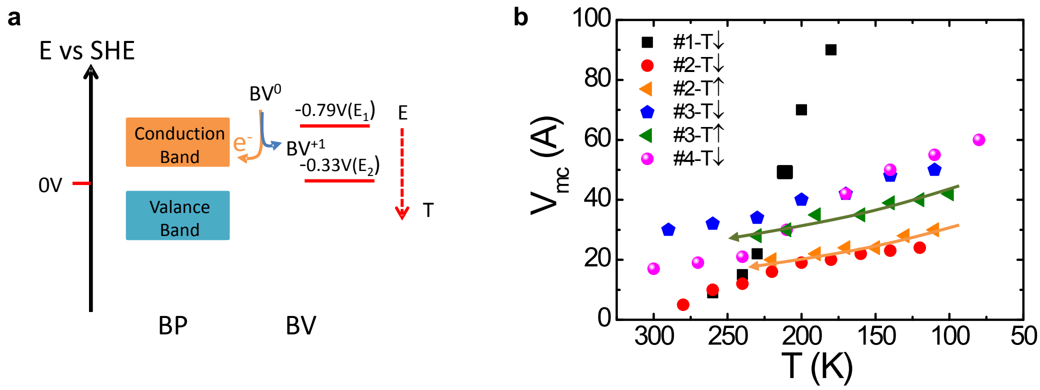

Figure S6 | a, BV reduction potential changes with temperature. b, V_{mc} is the voltage of minimum current. As the temperature is lowered, a clear shift of V_{mc} is observed from the different samples of #1, #2, #3, and #4. For the samples #2 and #3, we measured the output curves by heating to room temperature. We can see that when the temperature increases at low temperature region, this process is reversible. But, when temperature approaches room temperature, this process becomes irreversible, because the reduction potential changes and BV is damaged, as we demonstrated in the manuscript.

S7

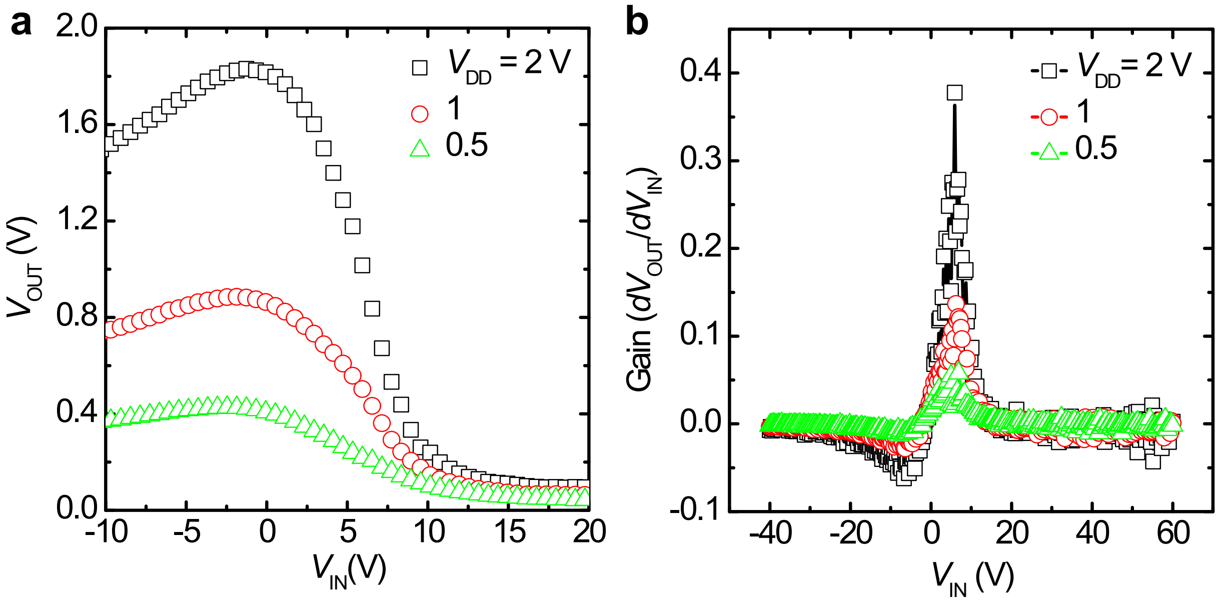

Figure S7 | The inverter characteristics of the BP device. a, The output voltage as a function of the input voltage. **b,** The inverter gain as a function of the input voltage.

Supplementary Note 1

Capping BP using h-BN

Capping BP using transparent h-BN effectively improved electron transport in BP devices relative to other techniques[2] by blocking acceptors generated from the air or environment. These effects rendered BP suitable for transparent photodetector and logical circuit applications. Few-layer BPs were transferred to a heavily p-doped silicon substrate capped with 300 nm thick SiO_2 according to the Scotch tape technique. Electron beam lithography and metal (Ti/Au of 20/50 nm) deposition were subsequently applied. We next used PDMS to stack h-BN onto the tops of the BP devices. The final device structure is depicted in **Figure S8a**, which shows the BP device capped with transparent h-BN. All measurements were carried out under vacuum using a semiconductor analyzer (Agilent 4155 C).

The device performances were initially measured prior to h-BN capping. The transfer characteristics of the pristine device (hBN1) are shown in Figure S8b. The excellent linear I_{ds}–V_{ds} curve suggested good contact between the metal electrodes and the BP flakes. Figure S8c presents the ambipolar transfer characteristics typical of h-BN-capped or pristine p-type BP devices. In contrast with the clear p-type transistor behavior, the red line reveals ambipolar characteristics, in which both electron and hole currents were observed. This transition was attributed to effective blocking of acceptors from the air and chemicals. At the equilibrium state, BP transistors always show p-type behavior. In order to enhance electron transport, h-BN was used to cap the BP devices and avoid introducing acceptors from air or environmental chemicals, such as H_2O or O_2, as shown Figure S8a. Thus, after transparent h-BN capping, the Fermi level was positioned closer to the conduction band than it was prior to treatment, indicating an improvement in the electron transportation. Ambipolar characteristics were obtained from the h-BN capped BP devices (hBN2, hBN3 are shown in **Figure 98**) as well, as summarized in a table listing the figures of merit of the h-BN capped BP devices in Table S4.

S8

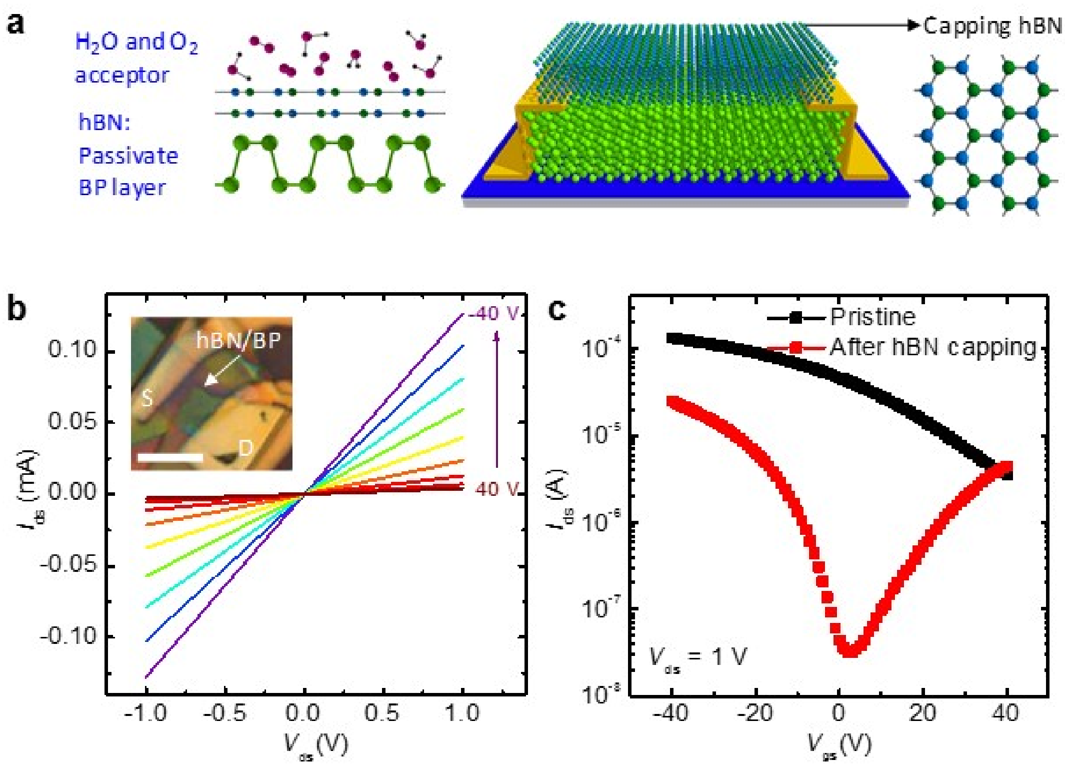

Figure S8 | The characteristics of the BP device. a, Hexagonal boron nitride (hBN)-encapsulated BP FET. The BP was protected from the ambient atmosphere by the hBN capping layer. **b,** Output curves obtained from hBN-capped devices, as a function of the gate bias. The clear linearity of the curves indicated Ohmic contact at the interface between the metal and the BP layer. The inset shows an optical microscopy image of the device. The scale bar indicates 5 µm. **c,** Transfer curves obtained from the pristine, hBN-capped BP devices. Ambipolar carrier transport was observed after hBN capping.

S9

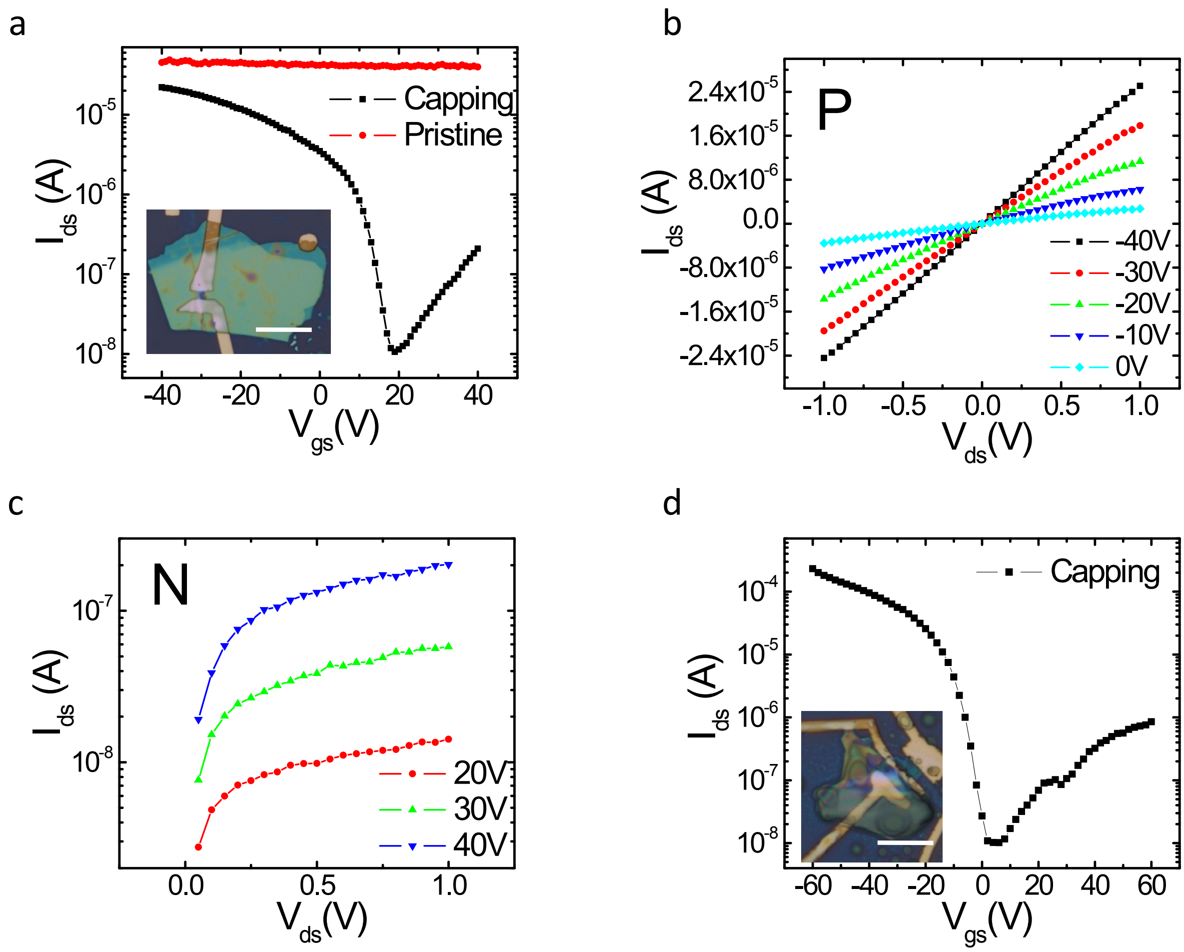

Figure S9 |a, shows ambipolar characteristic of h-BN capped BP devices (hBN2) and **b, c,** show output characteristics of the device (hBN2) in P- and N-type operations, respectively. **d,** shows ambipolar characteristic of h-BN capped BP devices (hBN3). The scale bar indicates 5 μm.

Table S4

Table S4 | Performance parameters of devices after hBN capping.					
	Mobility (cm^2/Vs)				
Samples*	**Pristine**	**After hBN capping**		**I_{On}/I_{off}**	**Thickness (nm)**
	Hole	**Hole**	**Electron**		
hBN1	156	68	20	10^3	8
hBN2	168	82	11	10^3	6
hBN3	350	339	8	10^2	13

* hBN# denotes the BP FET device fabricated by hBN capping.

References

1. D. Xiang, C. Han, J. Wu, S. Zhong, Y. Liu, J. Lin, X. A. Zhang, W. Ping Hu, B. Ozyilmaz, A. H. Neto, A. T. Wee and W. Chen, *Nature Communications*, 2015, **6**, 6485.
2. R. A. Doganov, E. C. O'Farrell, S. P. Koenig, Y. Yeo, A. Ziletti, A. Carvalho, D. K. Campbell, D. F. Coker, K. Watanabe, T. Taniguchi, A. H. Neto and B. Ozyilmaz, *Nature Communications*, 2015, **6**, 6647.
3. H. Liu, A. T. Neal, M. Si, Y. Du and P. D. Ye, *IEEE*, 2014, **35**, 795.
4. A. Avsar, I. J. Vera-Marun, J. Y. Tan, K. Watanabe, T. Taniguchi, A. H. Castro Neto and B. Özyilmaz, *ACS Nano*, 2015, **9**, 4138-4145.
5. W. Zhu, M. N. Yogeesh, S. Yang, S. H. Aldave, J.-S. Kim, S. Sonde, L. Tao, N. Lu and D. Akinwande, *Nano Letters*, 2015, **15**, 1883-1890.